PRESCREENING HYDRAULIC LIME-BINDERS FOR DISORDERED CALCITE IN CAESAREA MARITIMA: CHARACTERIZING THE CHEMICAL ENVIRONMENT USING FTIR

Yotam Asscher[1]* • Aliza van Zuiden[1] • Chen Elimelech[1] • Peter Gendelman[1] •
Uzi 'Ad[1] • Jacob Sharvit[1] • Michele Secco[2,3] • Giulia Ricci[2,4] • Gilberto Artioli[2,4]

[1]Israel Antiquities Authority, Jerusalem, Israel
[2]Inter-Departmental Research Center for the Study of Cement Materials and Hydraulic Binders (CIRCe), University of Padova, Italy
[3]Department of Cultural Heritage (DBC), University of Padova, Italy
[4]Department of Geosciences, University of Padova, Italy

ABSTRACT. Hydraulic lime binders are considered a technological marvel which revolutionized construction techniques in antiquity. The core material is made of a binder that is a mixture of calcite and hydraulic phases, which are amorphous silicate compounds that nanostructurally polymerize into insoluble phases that harden even underwater, formed during the reaction between lime and reactive silicates such as volcanic ash. This is also what makes hydraulic lime so hard to radiocarbon (^{14}C) date. These insoluble phases contain carbonates that may set centuries following their application, resulting in younger ages, which may contaminate the calcite fraction that is favorable for ^{14}C dating. This calcite fraction forms upon the incorporation of atmospheric carbon dioxide during the setting of the hydrated lime. Therefore, different characterization methods are being constantly developed for identifying and characterizing the components of hydraulic lime-binders. In this work, we present a rapid characterization technique based on Fourier transform infrared spectroscopy (FTIR) that characterizes the atomic disorder and chemical environment of the carbonates and silicates fractions in the binder. The atomic disorder of the calcite crystallites was determined by the ν_2 and ν_4 vibrational modes, and the silicates were characterized by the main peak asymmetry and full width at half maximum (FWHM). Different hydraulic binders from Caesarea Maritima were examined, including Herodian mortars from the underwater breakwater and on-land plasters and mortars from the port's warehouse and vaults. Hydraulic binders, in which the calcite fraction in the binder shows atomic disorder that is comparable to modern plaster binders, was associated with silicates that have asymmetry and FWHM of clays and quartz. These materials are considered to be in good preservation state for ^{14}C dating since their carbonates crystallites are disordered and did not interact with the environment chemically to form stable and ordered crystals. Interestingly, the atomic disord of binders that underwent chemical alterations and recrystallization processes, are associated with reactive silicates aggregates such as volcanic ash (pozzolana). These results suggest a new way to prescreen materials for radiocarbon dating based on the composition of lime-binders and preservation state of the carbonate fraction and hydraulic products.

KEYWORDS: atomic disorder, FTIR, grinding curves, hydraulic lime-builders.

INTRODUCTION

Radiocarbon (^{14}C) dating of lime-binders has the potential of resolving structural phases in cultural heritage. This is done by determining the age of the carbonate binder, which undergoes carbonation during the time of setting and hardening (Delibrias and Labeyrie 1964; Heinemeier et al. 2010; van Strydonck 2016). The carbonate binder is formed in a two-step reaction, that involves (1) hydrating quicklime, CaO, which is formed after burning carbonates to above 750°C, to form hydrated lime (Ca(OH)$_2$), which then (2) incorporates atmospheric CO$_2$ with its isotopic ^{14}C ratio to form microcrystalline calcite (Boynton 1980). In hydraulic lime-binders, chemical interactions between the binder and reactive aggregates change this simplified concept. Reaction processes between the reactive silicates that provide magnesium and aluminum ions into the lime alkalinic system, allows the formation of hydrated phases, such as the layered double hydroxides (LDH) hydrotalcite (Mg$_6$Al$_2$(OH)$_{16}$CO$_3$·4H$_2$O) and hydrocalumite (Ca$_4$Al$_2$(OH)$_{12}$(CO$_3$,OH)$_2$·4H$_2$O). These hydrated phases are poorly crystalline and may exchanges their carbonate content centuries following the lime-binder

---

*Corresponding author. Email: yotam.asscher@gmail.com.

application (Artioli et al. 2017; Ponce-Antón et al. 2018). Other insoluble phases are C-S-H, that hold the material strongly together, showing excellent mechanical properties, permeability and durability (Snellings et al. 2012; Secco et al. 2018). These C-S-H phases are paracrystalline calcic aluminosilicates, associated with pozzolanic reaction products and modern cement chemistry, commonly characterized by the absence of crystal-like long-range ordering (Snellings et al. 2012).

Characterizing lime-binders prior to ^{14}C dating helps identifying and purifying the carbonate fraction from contaminants, although requires rigorous laboratory procedures (Sonninen and Jungner 2001; Nawrocka et al. 2005; Lindroos et al. 2007; Marzaioli et al. 2014). A recent one suggests a multistep purification protocol based on particle size selection using wet sieving, with material characterization after each separation step (Addis et al. 2019). Characterizing the material allows to assess the presence of geological carbonates, which could increase the amount of dead carbon and push the date toward older ages. In hydraulic lime-binders, characterization also aims at identifying hydraulic reactions products that contain carbonates (such as LDH), which push the date toward younger ages. Alteration processes, such as recrystallization of the original calcite binder crystals, will also result in younger ages. Recrystallization processes may occur through Ostwald ripening, where a phase characterized by a more stable and more ordered crystal structure is formed through dissolution and reprecipitation processes (Lindroos et al. 2007; Artioli 2010; Miriello et al. 2010; Michalska and Czernik 2015; Ponce-Antón et al. 2018).

A rapid examination of the atomic order of calcites was developed based on peak shape analysis of spectra in transmission Fourier transform infrared spectroscopy (FTIR). The vibrational modes of calcite show sensitivity to the nature of formation and chemical environment, enabling to differentiate between pyrogenic plaster from geogenic limestone (Regev et al. 2010). This can be done by monitoring the IR peak shapes of the ν_3 ν_2 and ν_4 peaks, that are influenced both by particle size scattering effects in FTIR pellets and crystallites atomic disorder. Particle size related scattering processes causes peak narrowing as the particle sizes decrease, while the atomic disorder is related with peak broadening (Poduska et al. 2011). The method is therefore able to detect if the original crystals of plasters and lime-binders have interacted with the environment, to form stable phases through recrystallization processes. The new phases would be relatively ordered and deviate from the original plaster trendline (Regev et al. 2010). This method is named grinding curves, since the IR pellet is reground several times, showing a trend of IR peaks narrowing during the repeated grinding due to the decrease in particle size. This technique was applied on different materials, showing differences depending on nature and origin, including hydroxyapatite, aragonite and quartz (Asscher et al. 2011a, 2011b; Suzuki et al. 2011; Asscher et al. 2017; Toffolo et al. 2019). In quartz, the method was used to describe the differences in long range atomic order (crystallinity) between geological references of cryptocrystalline flint and a single crystal of quartz, based on the spectroscopic indicators of the silicate peak asymmetry and full width at half maximum (FWHM). FWHM probes atomic order since it represents the variability of the energy of the vibrational modes that depends on the atomic configuration. The asymmetry of the silicate peak characterizes the scattering effect on absorption bands. The asymmetric distribution with a tail at higher wavenumbers (positive asymmetry) points to a smaller contribution of scattering to absorption bands. A negative asymmetry (a tail toward lower wavenumbers) suggests the particles are large and scatter significantly (Asscher et al. 2017). In hydraulic lime-binders, the reactive silicate aggregates, hydraulic reaction products, inert silicates such as quartz and clays, and the binder calcite

matrix, all have different atomic disorder and are expected to follow similar trends as shown on references using these spectroscopic indicators.

In this work we apply the grinding curve method on hydraulic plasters and mortars from Caesarea Maritima, which some contains volcanic ash from Pozzuoli/Puteoli in the bay of Naples (Brandon et al. 2014). In Caesarea, plasters and mortars associated with water management were chosen for their hydraulic behavior, including the underwater breakwater of the harbor, and on-land water channels and roof insulation layers. Peak shape analysis of the carbonate fraction and associated silicate components was based on the references of calcite and quartz, to describe chemical alterations in hydraulic lime binders. The aim of this research is to assess the link between the binder preservation state, defined by the atomic disorder of the carbonate fraction, and the crystallinity at the atomic level of the associated silicates fraction. Results show a link between the carbonate preservation state and the nature of silicates hydraulicity, showing FTIR could be a promising tool to characterize the preservation state of samples prior to ^{14}C dating.

Historical and Archaeological Background

The city of Caesarea Maritima and its harbor Sebastos both were created as result of one of the more ambitious projects of Herod the Great between year 22 and 10/9 BCE (Josephus, BJ 1.414; JA 15.331-341).

In this article presented results of FTIR spectroscopy of the samples that were taken from the two major monuments created by Herod in Caesarea-Sebastos Harbor and the vaults below the High Platform of the Augustus and Dea Roma Temple.

The Sebastos harbor was investigated since the 1960s of the last century (Reinhard and Raban 2009). Two particular areas of the harbor were sampled—one of the underwater breakwater wooden caissons of the northern mole in the outer harbor (Area K), and the constructions of the terrestrial parts of the northern quay in the intermediate harbor (the port's warehouse or area LL) (Raban et al. 2009; 'Ad et al. 2018). The samples of the underwater breakwater (K-cast) and the samples from area LL (LL-5, 59, I and J) were taken from the construction phases belonging to the Herodian period.

The Augustus and Dea Roma Temple was, according to the description of Josephus, created "Directly opposite the harbor entrance, upon a high platform, rose the temple of Caesar, remarkable for its beauty and for its great size" (BJ 3.408-415). The remains of the temple and Temple Platform (Area TP) were first exposed during the late 1950s and extensively excavated since the 1990s by teams of CCE (Holum 2008; Stabler et al. 2008: 17–39) and of IAA (Porath 2008).

The preliminary results of the 2014–2019 project show that the construction by Herod the Great of the TP was comprised of two large (25.0×25.0 m) vaulted-structures to the north and south and group of the sixth smaller vaults in the middle. The central group was constructive link between the monumental staircase and the temenos area. The roofs of the vaults were covered with insulation layers of waterproof concrete (samples TP-6, TP-18 and TP-24). Their ceiling was used as a platform from where stairs led to the other areas of the temenos. The samples TP-18 and TP-23 are taken from original insulation layer and from an airshaft of the southern vaulted-structure, supposedly dated to the time of Herod. The samples TP-24 are taken from the insulation layer above and water installation

within the southern vaulted-structure respectively, both associated with the first century CE rearrangement. Sample TP-06 is of one of the latest isolation layers presumably dated to the Mid–Late Roman periods 150–300 CE. Two samples from plastered water channels were taken (TP-04 and TP-01), associated with the Roman 100 CE–300 CE, and Herodian 22 BCE–100 CE periods respectively.

MATERIALS AND METHODS

The city of Caesarea came into administrative importance and wealth during the rule of King Herod (37–4 BCE). During this time, innovative construction methods and materials were applied, including the addition of hydraulic/pozzolanic aggregates to lime mortars and casts of the underwater breakwater (Brandon et al. 2014). In this study, 11 samples of mortars and plasters were chosen and defined as hydraulic based on their visual appearance and hardness, and the contexts in which they were found, associated with water management (Table 1). The contexts include hydraulic lime-binders of the underwater breakwater, inner harbor, and vaults insulation layers that are associated with Herodian construction (Figure 1).

Fourier Transform Infrared Spectroscopy

Fourier transform infrared spectroscopy (FTIR) was carried out on the entire set of samples. About 1 mg of sample was ground in an agate mortar and pestle, then mixed with a few milligrams of spectro-grade potassium bromide. The powder was pressed in a Pike Press to produce 5-mm pellets. These pellets were analyzed at 4 cm^{-1} resolution using a Nicolet iS5 Fourier transform infrared spectrometer. The raw FTIR spectra are reported in the Supplementary Information online (Supplementary Figure S1). Several spectroscopic parameters, i.e. peaks intensity ratio, asymmetry relative to the peak maxima, and peak width, were calculated from each FTIR spectrum to monitor the peak shape and relative intensity variations among samples (Figure 2). Baseline information is available in Table 2. The carbonate peak analysis was following Regev et al. (2010). Although deconvolution is a preferable technique to isolate each single contribution of overlapping bands in FTIR analysis (Brangule et al. 2015), in this study, due to the nature of the main silicate peak that encapsulates multiple bands, the silicate peak analysis follow Asscher et al. (2017) to avoid smoothing or treatment of the data. The asymmetry and FWHM were calculated from the main peak, found between 900–1250 cm^{-1} (Table 2), to include all the different vibrational modes found in the silicate family (Farmer 1974).

In addition, several standards spectra available at the free FTIR library of the Kimmel Center for Archaeological Science were analyzed (http://www.weizmann.ac.il/kimmel-arch/infrared-spectra-library). In particular: clays (Montmorillonite-sodium SWY-1, Illite [#35 Illinois], Phlogopite-Ward's-45-V-1000-6-KBr, and Montmorillonite-Calcium [Arizona], feldspars (Oligoclase [Wards], Orthoclase-Pink-Ward's-45-V-1000-7-KBr, Albite [Wards, 72], Anorthite [Grass Valley, California, Wards]), glasses (Pyrex-1-9, Glass#4-Quartz, Obsidian [Wards], Opal [precious]), Quartz family (Quartz, Flint, Cristobolite [V10SH]), volcanic materials (Tuff volcanic from Mt. Bental Golan Heights, Pumice [Tel Dor Area H Iron Age], Pozzolana [Bacoli, Pozzuoli; P. Tiano]) and igneous materials (Diorite-Ward's-45-E-3100-10-KBr, Basalt from Chispin, Israel, Olivine [San Carlos, Arizona, Wards], Periodite-Ward's-45-E-3100-12-Kbr).

Table 1 Hydraulic plasters and mortars presented in this study coming from Caesarea.

| Sample	Locus	Context	Visual description of aggregates	Proposed historical period
TP-01	L10680	Water channel, inside vault 1	Local sandstone, seashells	Roman 100 CE–300 CE
TP-04	L10666	Water channel, in front of port's vault 1	Local sandstone, glassy materials	Herodian 22 BCE–100 CE
TP-06	L15005	Isolation layer nr.2, on top of the vaults 3 and 4	Wood ash, local sandstone, seashore materials, seashells	Mid–Late Roman periods 150–300 CE
TP-18	L15008	Isolation layer nr.6, on top of the vaults 3 and 4	local sandstone, volcanic materials, wood ash	Herodian 22 BCE–100 CE
TP-23	L15009	Airshaft, in vault 1, eastern wall	Local sandstone, seashells, wood ash, limestone	Herodian 22 BCE–100 CE
TP-24	L15007	Isolation layer nr.5 (transitional layer) on top of the vaults 3 and 4	Sporadic limestone, volcanic materials, wood ash	Early Roman A layer following the Herodian layer (TP-018)
LL-5	W2010	Foundation of inner eastern wall, between room R–1/R–5, port's warehouse area	Local sandstone, seashells, wood ash, limestone	Herodian 22 BCE–100 CE
LL-59	W993	Quay of the intermediate harbor, port's warehouse area	Local sandstone, volcanic materials	Herodian 22 BCE–100 CE
LL-I	W994	Quay of the intermediate harbor, port's warehouse area	Local sandstone, volcanic materials	Herodian 22 BCE–100 CE
LL-J	W996	Additional wall on the intermediate harbor showing metal clamps, port's warehouse area	Seashells, wood ash, volcanic materials	Herodian 22 BCE–100 CE
K-cast	L102	Mortar found in the wooden caisson, at the outer harbor underwater breakwater	Local sandstone, volcanic materials	Herodian 22 BCE–100 CE
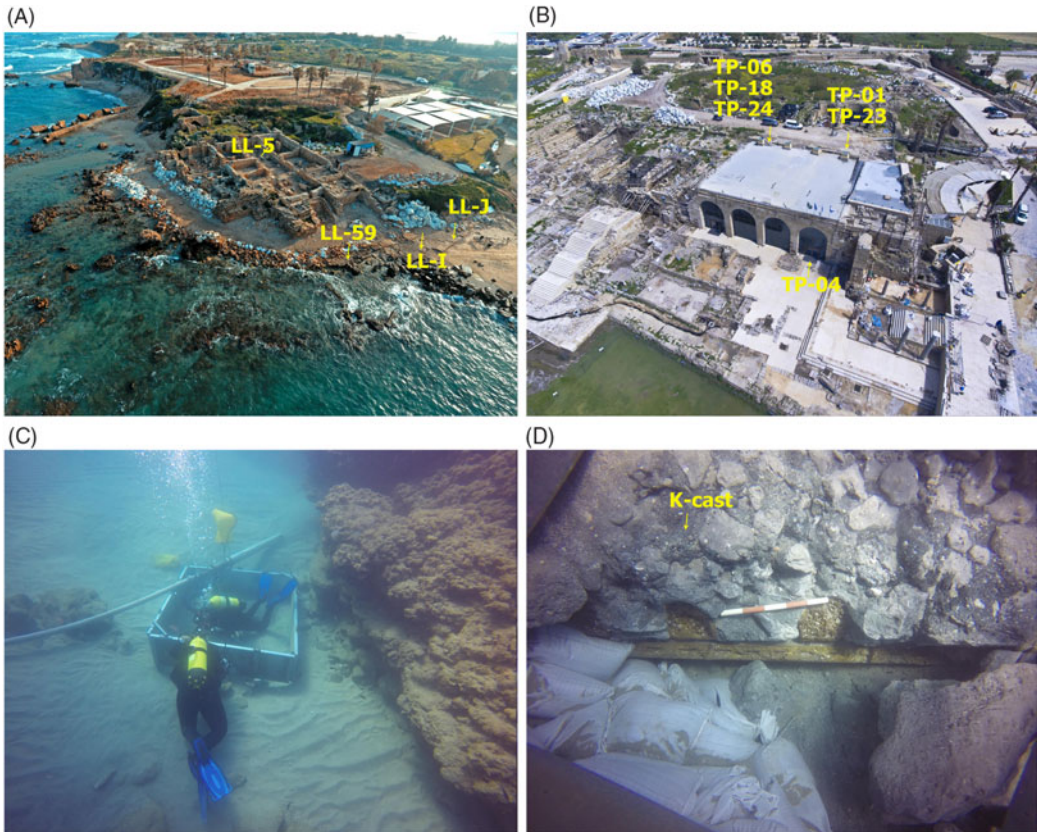
Figure 1   Areas of sampling in Caesarea Maritima: area LL in the port's warehouse area at the intermediate harbor (A), area TP in the port's vaults (B), and area K at the outer harbor (C). Arrows point to the location of samples. The underwater breakwater of area K is showing also the wooden caisson and place of sampling (D).
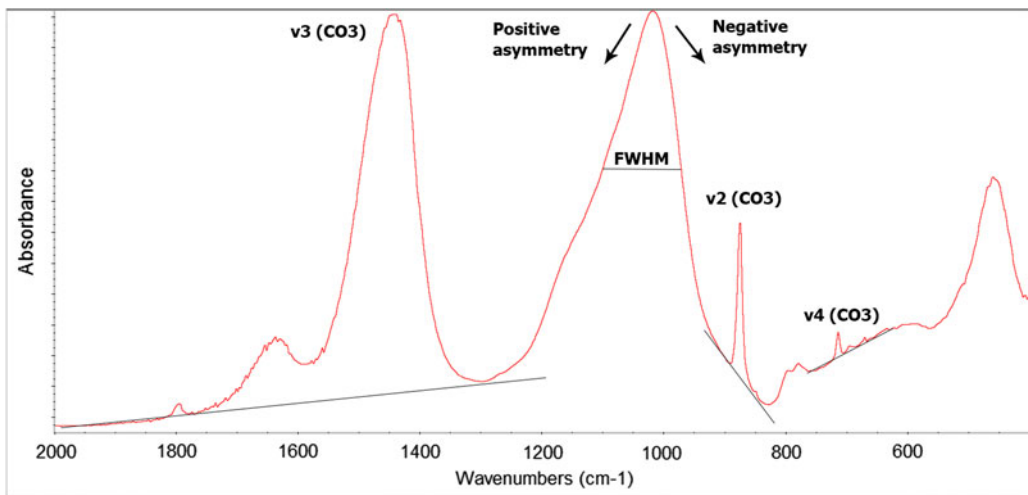

Figure 2   Spectroscopic indicators that were monitored in this study. The carbonate peak analysis of the ν_3, ν_2 and ν_4 peak heights follow Regev et al. (2010). The silicate peak FWHM and asymmetry following Asscher et al. (2017).

Table 2 Peak positions and baselines of vibrational bands used to calculate peaks intensity, asymmetry and width. For each peak the baseline is defined by two points selected at the local minimum in the spectral region here indicated (Figure 2). *The baseline of the ν_2 and ν_4 follow Chu et al. (2008).

Vibrational mode	Vibrational mode maximum peak position (cm^{-1})	Baseline (cm^{-1})
ν_3 (CO$_3$)	1425	2000–1800/1400–1200
ν_2 (CO$_3$)	875	1000–900/900–800*
ν_4 (CO3)	712	770–710/710–600*
Silicate main peak FWHM	900–1250	1400–1200/900–700
Silicate main peak asymmetry	900–1250	1400–1200/900–700

X-Ray Fluorescence

X-ray fluorescence (XRF) was carried out on all 11 samples. About 3 g of sample was ground in an agate mortar and pestle, then sieved through a 500-μm mesh, and placed in a Bruker sample cups and covered with a layer of Prolene roll. XRF analyses were carried out using a Bruker 5i Tracer handheld energy dispersive XRF spectrometer. The instrument is equipped with a Rh-anode, miniaturized X-ray tube operating at a maximum voltage of 50 kV and with a Peltier-cooled high-resolution silicon drift detector (SDD). The diameter of the X-ray spot on the sample is about 7–8 mm and accurate positioning on the point to be analyzed is obtained by means of an integrated camera. The raw XRF spectra are reported in the supplementary information online (Supplementary Figure S4). The quantifications of elements were provided by the instrument software, based on built-in calibrations, and published elsewhere (Rowe et al. 2012). In order to compare different samples, the semi-quantified net counts of the different elements were converted to oxides via the conversion table of the James Cook University of Australia. The hydraulic index (HI), following Vola et al. (2011), was used to estimate the hydraulicity of the sample following the equation: $H1 = \frac{SiO_2 + Al_2O_3 + Fe_2O_3}{CaO + MgO}$

This calculation sums the contribution of the elemental composition of the hydraulic components of the binder and the aggregates, as a bulk analysis. Therefore, it is suitable for comparison with the FTIR spectra of the same powders, which provide information on the bulk mineralogical composition.

X-Ray Powder Diffraction

Mineralogical quantitative phase analyses (QPA) were performed on selected hydraulic plasters through X-ray powder diffraction (XRD). The analyses were carried out after grinding the obtained powder with an agate mortar. Data were collected using a Bragg–Brentano θ-θ diffractometer (Malvern Panalytical X'Pert PRO, Co Kα radiation, 40 kV and 40 mA) equipped with a real time multiple strip (RTMS) detector (X'Celerator by Malvern Panalytical). Divergence and anti-scattering slits, of ¼° and ½° respectively, were mounted in the incident beam pathway. The pathway of the diffracted beam included a soller slit (0.04 rad) and antiscatter blade (5 mm). Data acquisition was performed by operating a continuous scan in the range 3–90 [°2θ], with a virtual step scan of 0.02 [°2θ]. Diffraction patterns were interpreted with X'Pert HighScore Plus 3.0 software by Malvern Panalytical, qualitatively reconstructing mineral profiles of the compounds by comparison
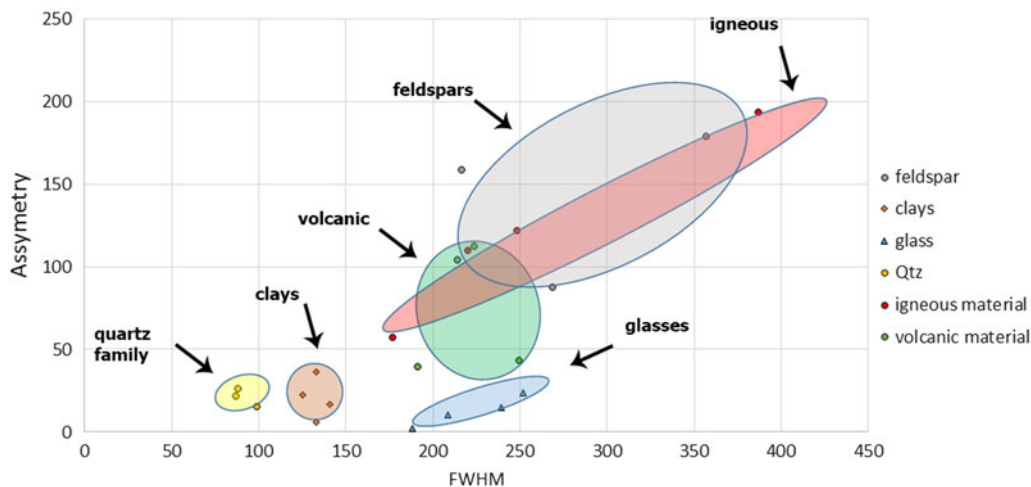
Figure 3   FTIR spectroscopic indicators of asymmetry and FWHM of silicates standards. Note that quartz and clays are at one end of the trendline, showing lower values of asymmetry and FWHM. Feldspars, glass, volcanic materials and igneous materials are toward higher asymmetry and FWHM values.

with PDF databases from the International Centre for Diffraction Data (ICDD). The raw XRD patterns are reported in the Supplementary Information online (Supplementary Figure S5). Then, QPAs were performed using the Rietveld method (Rietveld 1969). Refinements were accomplished with TOPAS software (version 4.1) by Bruker AXS. The observed Bragg peaks in the powder patterns have been modelled through a pseudo-Voigt function, fitting the background by a 12 coefficients Chebyshev polynomial. For each phase, the lattice parameters, Lorentzian crystal sizes and scale factors have been refined. During the refinement, any residual preferred orientation effect was modelled with the March Dollase algorithm (Dollase 1986). The starting structural models for the refinements were taken from the International Crystal Structure Database (ICSD).

RESULTS

FTIR spectra of selected standards of silicates, including different clays, feldspars, glass, quartz, volcanic materials and igneous materials were examined for their silicate's crystallinity at the atomic level (Figure S2). A clear trend toward higher values of FWHM and asymmetry of the main silicate peak is observed for materials of volcanic or igneous origin (Figure 3). In general, volcanic and igneous rocks show higher polycrystallinity which is reflected in higher asymmetry values, and since they were formed in high pressure and temperature conditions, their crystallinity at the atomic level is lower, reflected in higher FWHM. As expected, the quartz family shows higher atomic crystallinity, being at the far end with lower FWHM values. Glasses, clays and the quartz family have similar asymmetry values, indicating comparable scattering effects on the absorption bands (Asscher et al. 2017). This is due to similar chemical formula and particle size distributions, although their crystallite size within the particles differentiates significantly. Glasses are clearly distinct due to their internal atomic disorder (amorphous material), which shows higher FWHM. Interestingly, feldspar minerals show a large variability, related with high asymmetry and FWHM values. This can be attributed to the difficulty in estimating asymmetry, due to the multiple sharp peaks in the silicate range (Figure S2). Volcanic and igneous materials are a composition of several
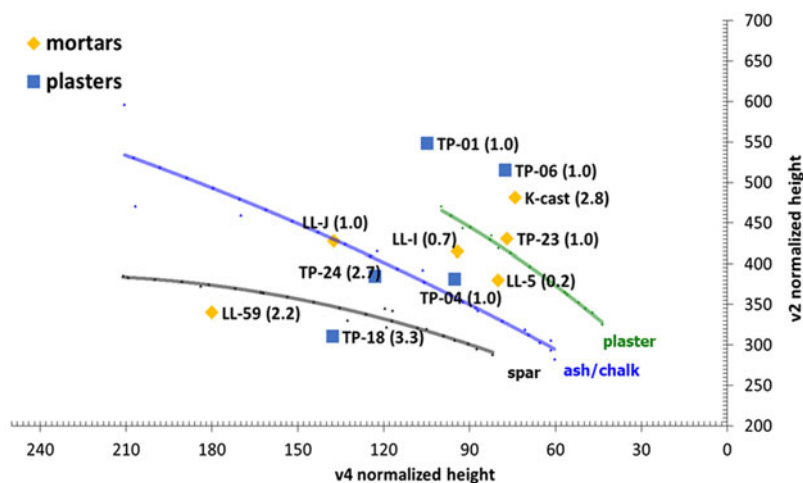
Figure 4 FTIR spectroscopic indicators of the calcite ν_2 and ν_4 vibrational modes peak heights (normalized to ν_3) of mortars and plasters from Caesarea. Noted also is the hydraulic index as calculated from elemental composition following Vola et al. (2011) (in brackets).

minerals, which would also influence the estimation of the FWHM and asymmetry, however, the general trend is maintained through these composite materials. The spectroscopic indicators FWHM and asymmetry can be used to describe the silicate materials crystallinity, and this information is used to estimate the silicate fraction in the hydraulic lime-binders in Caesarea.

The carbonate fraction peak shape analysis of hydraulic lime-binders in Caesarea (samples in Table 1) shows that not all of the samples contain calcite crystals that retain their original atomic disorder. References of modern plaster (green), chalk or ash calcite crystals (blue), and geological calcitic spar (black) (based on Regev et al. 2010), illustrates well the shift of some hydraulic calcitic binders towards geological atomic disorder (Figure 4). The calcite normalized heights in Figure 4 are by dividing the ν_2 and ν_4 vibrational modes with the main peak ν_3 (shown in Figure 2). Visual observations of the aggregates show that the local sandstone (namely Kurkar), seashells, wood ash and volcanic materials were mainly used, with sporadic observations of limestone aggregates. The limestone would influence the grinding curve if small fractions were to be included in the binder sample for FTIR (sieved with a 500-μm mesh), however, the samples in which limestone was observed (Table 1), are not shifted towards geological references in the grinding curve plot (Figure 4). The mortars and plasters that show atomic disorder that is similar or higher than modern plaster, namely TP-01, TP-06, K-cast and TP-23, are considered preserved atomically since their crystallites have not recrystallized to form a more ordered phase. During the process of recrystallization, the carbonate ions interact chemically with the environment through pore water dissolution and reprecipitation processes, which influences the original ^{14}C signal. Sample TP-06 shows the presence of aragonite (see Figure S1), based on the shift of the ν_2 vibrational mode from 875 cm^{-1} to 856 cm^{-1} (Farmer 1974), and a correction for the intensity of the ν_4 peak height was used based on XRD data, following Toffolo et al. (2019). Aragonite is reported as an alteration product of C-S-H cementitious binders in hydraulic mortars (Jackson 2014), however, visual observations of shells suggest that the shells aragonite crystal fragments were mixed in the powder

subsample. The other samples show the carbonate fraction somewhat deviates towards the atomic disorder of geological references (towards the spar reference). This could be explained in three ways: (1) the sample powder contains enough geological materials such as limestone aggregates, that could not be eliminated during the sample preparation, (2) the carbonate binder recrystallized overtime, showing higher atomic order through Oswald ripening, and (3) presence of LDH phases that may influences the interpretation.

To check if the binder atomic disorder is influence by hydraulicity and LDH phases, chemical composition was measured using XRF. The HI can estimate the chemical potential for the formation of hydrated phases and hydraulic products (Vola et al. 2011), based on the equation: $H1 = \frac{SiO_2 + Al_2O_3 + Fe_2O_3}{CaO + MgO}$. The elemental composition of magnesium (Mg), calcium (Ca), silicon (Si), iron (Fe) and aluminum (Al), were measured using XRF and semi-quantified based on an internal calibration following homogenization (Rowe et al. 2012). It is important to note that the same powders for XRF were also used for FTIR measurements. Plotting the HI values (in brackets, Figure 4) shows that there is a pattern between the atomic disorder of the calcitic binders and hydraulicity. The samples with HI index > 2 are associated with atomic disorder of geological references in the grinding curve plot (including LL-59, TP-18 and TP-24). One exception was found, which is the sample from the underwater breakwater (K-cast). This sample shows high HI index (2.8), and high atomic disorder. This could be related with the fact it was set underwater, where the chemistry of hydrated phases is different due to the chemical environment (Jackson et al. 2017). The samples that are between the plaster and ash/chalk trendlines show HI index that ranges between 0.2–1 (including LL-5, LL-I, LL-J and TP-04). To understand better the relations between hydraulicity and the atomic disorder of the binder's calcitic crystallites, we examined the FWHM and asymmetry of the silicates fraction in the FTIR spectra.

We differentiate between highly preserved samples (showing calcite crystallites atomic disorder above the plaster line, namely TP-01, TP-06, LL-cast and TP-23), slightly altered (between the plaster and ash/chalk lines, namely LL-I, LL-J, LL-5 and TP-04) and strongly altered (below the ash/chalk line, namely TP-24, TP-18 and LL-59). We plotted the mortars and plasters according to their calcitic binder preservation state on the plot that describes that silicate crystallinity at the atomic level (Figure 5), using all three IR measurements of the same sample following the grinding curve method. Results show a neat trend in which the samples with highly disorder calcite (above the modern plaster line in Figure 4), are associated with silicates that have low asymmetry and FWHM (similar to those of clays and quartz). The grinding curves analysis shows that changes in particle size scattering effect does not change significantly the overall understanding in asymmetry and FWHM trends. The third ground in each grinding curve, which correlates with the narrowest FTIR peaks, scatters nicely (in Figure 5A, the third ground is marked with a cross), and the three measurements in the grinding curves of samples TP-06, TP-18 and TP-24 are well grouped (Figure 5B). This shows that a single measurement, well grounded, can be used to obtain the general trend.

Interestingly, the calcitic binder that is considered strongly altered, due to the deviation from modern plasters towards geological references, correlates well with silicates having higher atomic disorder (such as volcanic materials). The silicates atomic crystallinity provides evidence to the presence of hydraulic aggregates and products. This implies that the poorly ordered phases that are formed during hydraulic reactions influence greatly the calcite in the binder, and that this can be detected using FTIR. These poorly ordered phases, such as the LDH's hydrotalcite and hydrocalumite, are phyllosilicates characterized by a flexible layered
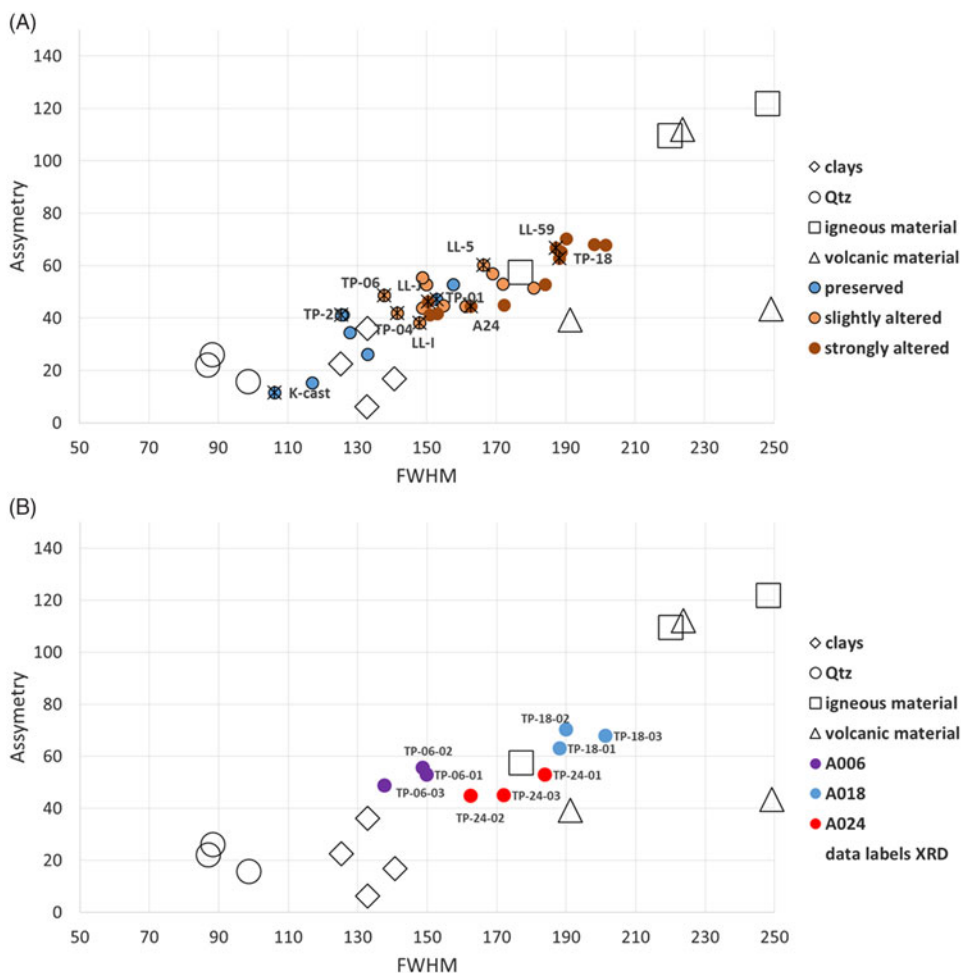
Figure 5   FTIR spectroscopic indicators of asymmetry and FWHM of silicate standards and hydraulic plasters and mortars from Caesarea. 5A) Repeated grinding of preserved materials, slightly and strongly altered (based on their calcite atomic disorder). Quartz (empty circles) and clays (empty diamonds) overlap with preserved materials, while the strongly altered overlap with the igneous (empty squares) and volcanic materials (empty triangles). An internal cross within the full circles represents the third ground in each grinding curve. 5B) Spectroscopic indicators of asymmetry and FWHM of silicate standards and samples TP-06, TP-18 and TP-24. Note that TP06 is overlapping the silicate crystallinity area of clays, while TP-24 and TP-18 are towards the ranges of volcanic materials and igneous rock, which is in agreement with the material mineralogical composition as determined by XRD (Table S2). Repeated grinding steps are marked in the label of the sample.

structure prone to dynamic exchanges of carbonate anions derived from atmospheric CO_2 (Conterosito et al. 2018). The binder is a mixture of calcite and hydraulic phases indiscriminately, therefore, the enhanced ionic exchanges of the hydraulic phases may promote recrystallization processes in the calcitic fraction it is in contact with.

To understand if the silicate crystallinity plot is related with reactive silicate and hydraulic products, three plasters and one mortar were sub–sampled for XRD measurements. XRD enables to quantify the mineralogical composition and estimate the relative amount of poorly

Table 3 Samples XRD phases are analcime (ana), biotite (bio), calcite (cal), gypsum (gyp), laumontite (laum), philipsite (phil), plagioclase (plag), quartz (qtz), sanidine (san), smectite (sme), aragonite (ara), and amorphous components (amp). The silicates to carbonates ratio in XRD is defined by the ratio between the QPA analysis values of (ana+bio+laum+phil+plag+qtz+san+smec) divided by (cal+ara). Also noted are the HI index based on XRF, and the FTIR spectra peak ratio between the major peak of the silicates and the major peak of the carbonates. It is important to note that the relative peak intensities in FTIR, XRF and XRD are affected by different factors, and are not a direct indication of the relative proportions of these phases.

Sample	Mineralogy (XRD)	HI (XRF)	Silicates to carbonates ratio (FTIR)	Silicates to carbonates ratio (XRD)
K-cast	ana, bio, cal, gyp, laum, phil, plag, qtz, san, sme, amp	2.8	6.5	8.5
TP-06	cal, plag, qtz, san, sme, ara, amp	1.0	0.4	0.3
TP-18	ana, bio, cal, laum, phil, plag, qtz, san, sme, amp	3.3	1.3	3.9
TP-24	ana, bio, cal, gyp, laum, phil, plag, qtz, san, sme, amp	2.7	0.7	1.2

crystalline (or amorphous) hydraulic phases. Quantitative phase analysis (QPA) shows that the underwater sample from the breakwater (K-cast) contains non-reactive silicates such as smectite from the clay family, and reactive silicates from volcanic origin, based on the presence of analcime, laumontite and philipsite minerals that are part of the zeolite group, commonly found in volcanic materials (Table S2). The presence of volcanic materials is in agreement with previous studies on the mortars from Caesarea Maritima breakwater (Jackson et al. 2017).

When comparing the ratios between the amount of silicates and carbonates found in the samples, we see a general trend between the silicates to carbonates ratio in QPA analysis (based on XRD), the HI index (based on XRF) and the ratio between the major peaks in FTIR spectra of the silicates (around 1050 cm^{-1}) and the carbonates (around 1425 cm^{-1}). High values of HI (indicating hydraulicity following Vola et al. 2011) is marked with high values of silicates to carbonates ratio based on QPA and FTIR (Table 3). The correlation between chemical composition (XRF) and mineralogy (XRD and FTIR) show it is possible to identify hydraulic lime-binders using FTIR, and that the repeated grinding does not change significantly the interpretation.

Interestingly, the on-land samples from the vaults insulation layers (TP-18 and TP-24) show similar compositions, indicating they were made from the same materials, perhaps from the volcanic ash that was brought from Italy (Brandon et al. 2014), but with much less clays. These insulation layers are both associated with Herodian or early Roman technology (Table 1). We note that the insulation layer that is associated with Mid–Late Roman period (TP-06) shows a different composition, with calcite, quartz and aragonite (from shells that are observed visually) as major constitutes, which implies that there was a change in Roman technology during that time. In addition, the plasters from on-land structures also shows striking similarity with the underwater breakwater mortars, based on phase composition (XRD), hydraulicity (XRF) and FTIR peak shapes. This result suggests that the reactive silicates that were used for the construction of the harbor, perhaps the

pozzolana from Italy (Brandon et al. 2014), were incorporated in the construction process of other structures and functions on land.

DISCUSSION

[14]C dating of archaeological lime-binders deviate from the true age due to contaminates, especially in the case of pozzolanic/hydraulic mortars (Ringbom et al. 2014; Michalska 2019). This is also true for pure lime-binders, presumably due to residual geogenic or secondary carbonates (Folk and Valastro 1976). Therefore, ^{14}C dating of plasters and mortars is still showing varying protocols between laboratory procedures with few applications (Zouridakis et al. 1987). Acid hydrolysis, being a popular protocol in dating lime-binders, is based on sequential dissolution of the carbonate binder. This protocol improved the applications, in particular when combined with sample prescreening and the introduction of accelerator mass spectrometry (AMS) (Heinemeier et al. 1997; Lindroos et al. 2007). Overall, ^{14}C dating of lime-binders has so far proven a difficult with irreproducible results due to the occurrence of a number of contaminants embedded within the calcitic fraction in the binder (Regev et al. 2011; Hajdas et al. 2017; Hayen et al. 2017). Here we show that by characterizing hydraulic lime-binders, it is possible to identify the phases that contaminate the calcitic fraction, including recrystallized calcite crystals and the hydraulic products.

FTIR measurements provide information on the chemical environment of lime-binders components, through peak shape analysis. Semi-quantified spectroscopic indicators provide information on the carbonate and hydraulic fractions of the binder in the same spectrum. The carbonate fraction, which is the one suitable for radiocarbon dating, is characterized by the calcite ν_2 and ν_4 vibrational modes and their relative heights, which are correlated with atomic disorder (Poduska et al. 2011). Moreover, in cases that the binder includes a carbonate fraction and hydraulic components, the silicates main peak FWHM and asymmetry characterizes the aggregates and products hydraulicity. In Caesarea, hydraulic mortars and plasters were characterized, and peak analysis of the carbonates and silicates was compared with standard references of calcite and silicates of different origin and atomic disorder. In general, the calcitic binders that show higher atomic disorder are associated with pristine crystallites, which are suitable for ^{14}C dating. These crystallites did not recrystallize over time, and they were found to be associated with silicates that have higher atomic order (quartz, clays). Altered calcitic binders, i.e. calcite crystallites with higher atomic order which suggests recrystallization processes occur, were found associated with silicates of higher atomic disorder (volcanic materials). These results were corroborated by chemical composition based on XRF and the estimation of the sample's hydraulicity, and mineralogical phases quantification based on XRD.

One application for this study could be a rapid prescreening method for materials for radiocarbon dating. Rigorous sample preparation (Addis et al. 2019) and mineralogical phases quantification after each step in the purification process is time consuming, which may result in samples that are not suitable for further processing. A rapid examination using FTIR could exclude samples based on their mineralogical atomic order, showing calcites atomic disorder and their associated silicates in hydraulic lime-binders. Silicates in hydraulic binders suggest LDH phases, which may influence the radiocarbon date (Artioli et al. 2017). Rapid and low cost FTIR measurements should be useful in the screening process on site, as this technique is transportable and complementary with a handheld portable XRF. The results would imply if the binder's calcitic fraction is preserved or it has recrystallized. The FTIR measurements

would also provide information on the hydraulicity, and the presence of LDH phases which would push ^{14}C ages toward younger ages. Moreover, this general characterization would upgrade the toolkit of radiocarbon specialized laboratories that do not have large scale facilities to study the materials (such as XRD and SEM-EDS), and sometime get from archaeologists only low amounts of materials (which is suitable for FTIR measurements).

The limitations of a rapid prescreening method is mainly related with the sampling strategy. Sampling binder powders sieved through 500 μm mesh may include small aggregates particles that influence the mineralogical analysis of the FTIR and chemical analysis of the XRF. Since limestone aggregates were rare in the mortars and plaster in Caesarea, the atomic disorder of the binder was correlated with recrystallization processes, in cases the grinding curves were in the geological region. Therefore, this method is suitable for rapid examinations of the calcitic binder atomic crystallinity in Caesarea, a key component in choosing samples for radiocarbon dating. This could be more difficult in areas where limestone was commonly used as aggregate. To improve the sampling strategy, one would have to go through wet separation of the binder (Addis et al. 2019), which identifies and then removes geological aggregates, lime lumps, and recrystallized calcite based on density and centrifugation steps. Wet separation is reported to contain more amorphous phases, such as LDH and C-S-H, compared with bulk analysis, which is favorable for radiocarbon dating (Addis et al. 2019). Looking into the atomically disordered calcitic fraction of wet separated fractions, compared with bulk 500 μm sieved powders, FTIR examinations of hydraulic materials from Cannero, Italy (Ricci et al. 2020 in this issue), show a clear trend towards pristine and disordered crystallites in the wet fraction, based on the grinding curve plot of calcites (Figure S3A). The materials were hydraulic showing large FWHM and asymmetry peak shape analysis (Figure S3B), supported by XRD examinations (Figure S3C), which help in the radiocarbon dating process.

CONCLUSIONS

Prescreening hydraulic lime-binders prior to ^{14}C dating, based on FTIR mineralogical analysis, is shown on samples from Caesarea Maritima. The atomic disorder of the calcite crystallites in the binder's matrix, and the associated silicates in hydraulic aggregates and reaction products can be assessed from FTIR peak shapes analysis. The atomic disorder of calcite enables distinguishing between recrystallized calcite from pristine original crystals, which is crucial for choosing the relevant samples for radiocarbon dating. The atomic disorder of the silicates describes the hydraulicity of the binder. This is achieved by monitoring the ν_2 and ν_4 vibrational modes of calcite, and the silicates main peak asymmetry and FWHM. Interestingly, the recrystallized samples were associated with higher hydraulicity, supported by XRF and XRD measurements. Characterizing lime-binders for radiocarbon dating is a crucial step in sample selection, which will allow excluding samples with contaminations such as limestone aggregates, and LDH phases. Finding the correlation between recrystallized calcite in the binder and hydraulic components, based on FTIR measurements, contributes to the understanding of this complex material. Applying these methods in characterizing the materials prior to dating will improve the toolkit in radiocarbon laboratories and help explain ambiguous results, through rapid examinations on-site.

ACKNOWLEDGMENTS

writing the paper. We also thank the reviewers for their comments, which improved the paper significantly.

SUPPLEMENTARY MATERIAL

To view supplementary material for this article, please visit https://doi.org/10.1017/RDC.2020.20

REFERENCES

'Ad U, Arbel Y, Gendelman P. 2018. Caesarea, Area LL. HA-ESI 130 (July 16). http://www.hadashot-esi.org.il/report_detail_eng.aspx?id=25450&mag_id=126 [accessed July 31, 2019].

Addis A, Secco M, Marzaioli F, Artioli G, Arnau AC, Passariello I, Terrasi F, Brogiolo GP. 2019. Selecting the most reliable ^{14}C dating material inside mortars: The origin of the Padua Cathedral. Radiocarbon. 61(2):375–393. doi: 10.1017/RDC.2018.147.

Artioli G. 2010. Scientific methods and cultural heritage. Oxford University Press.

Artioli G, Secco M, Addis A, Bellotto M. 2017. Role of hydrotalcite-type layered double hydroxides in delayed pozzolanic reactions and their bearing on mortar dating: composition, properties, application. In: Herbert P, editor. Cementitious materials: composition, properties, application. Berlin: Walter de Gruyter GmbH. 500 p.

Asscher Y, Weiner S, Boaretto E. 2011a. Variations in atomic disorder in biogenic carbonate hydroxyapatite using the Infrared spectrum grinding curve method. Advanced Functional Materials, 21(17):3308–3313.

Asscher Y, Regev L, Weiner S, Boaretto E. 2011b. Atomic disorder in fossil tooth and bone mineral: an FTIR study using the grinding curve method. Archaeoscience 35:135–141.

Asscher Y, Dal Sasso G, Nodari L, Angelini I, Ballaran TB, Artioli G. 2017. Differentiating between long and short range disorder in infrared spectra: on the meaning of "crystallinity" in silica. Physical Chemistry Chemical Physics 19(32):21783–21790.

Boynton RS. 1980. Chemistry and technology of lime and limestone. New York: John Wiley & Sons, Inc.

Brandon CJ, Hohlfelder RL, Jackson MD, Oleson JP, editors. 2014. Building for eternity: The history and technology of Roman concrete engineering in the sea. Oxford: Oxbow Books.

Brangule A, Gross KA. 2015. Importance of FTIR spectra deconvolution for the analysis of amorphous calcium phosphates. IOP Conf. Ser. Mater. Sci. Eng. 77: 012027.

Chu V, Regev L, Weiner S, Boaretto E. 2008. Differentiating between anthropogenic calcite in plaster, ash and natural calcite using infrared spectroscopy: implications in archaeology. Journal of Archaeological Science 35:905–e911.

Conterosito E, Gianotti V, Palin L, Boccaleri E, Viterbo D, Milanesio M. 2018. Facile preparation methods of hydrotalcite layered materials and their structural characterization by combined techniques. Inorganica Chim Acta. 470:36–50. doi: 10.1016/j.ica.2017.08.007.

Delibrias G, Labeyrie J. 1964. Dating of old mortars by the carbon-14 method. Nature 201.

Dollase WA. 1986. Correction of intensities for preferred orientation in powder diffractometry: application of the March model. Journal of Applied Crystallography 19:267–72.

Farmer VC. 1974. The infrared spectra of minerals. London: Mineralogical Society.

Folk RL, Valastro S. 1976. Successful technique for dating of lime mortar by Carbon-14. Journal of Field Archaeology 3(2):203–208.

Hajdas I, Lindroos A, Heinemeier J, Ringbom Å, Marzaioli F, Terrasi F, Passariello I, Capano M, Artioli G, Addis A, et al. 2017. Preparation and dating of mortar samples—Mortar Dating Intercomparison Study (MODIS). Radiocarbon 59(5):1–14.

Hayen R, Van Strydonck M, Fontaine L, Boudin M, Lindroos A, Heinemeier J, Ringbom Å, Michalska D, Hajdas I, Hueglin S, et al. 2017. Mortar dating methodology: Assessing recurrent issues and needs for future research. Radiocarbon 59(6):1859–71.

Heinemeier J, Jungner H, Lindroos A, Ringbom Å, von Konow T, Rud N. 1997. AMS ^{14}C dating of lime mortar. Nuclear Instruments and Methods in Physics Research B 123:487–495.

Heinemeier J, Ringbom Å, Lindroos A, Sveinbjörnsdóttir ÁE. 2010. Successful AMS ^{14}C Dating of Non–Hydraulic Lime Mortars from the Medieval Churches of the Åland Islands, Finland. Radiocarbon. 52(1):171–204.

Holum KG. 2008. Caesarea. The combined Caesarea Expedition excavations. In: Stern E, Geva H, Paris A, editors. The new encyclopedia of archaeological excavations in the Holy Land. Supplement Vol. 5. Jerusalem. p. 1665–1668.

Jackson M. 2014. Sea-water concretes and their material characteristics. In: Building for eternity. Oxford: Oxbow Books. p. 141–187.

Jackson MD, Mulcahy SR, Chen H, Li Y, Li Q, Cappelletti P, Wenk HR. 2017. Phillipsite and Al-tobermorite mineral cements produced through low-temperature water-rock reactions in Roman marine concrete. Am Mineral. 102(7):1435–1450. doi: 10.2138/am–2017–5993CCBY.

Lindroos A, Heinemeier J, Ringbom Å, Braskèn M, Sveinbjörnsdóttir Á. 2007. Mortar dating using AMS ^{14}C and sequential dissolution: examples from medieval, non-hydraulic lime mortars from the Aland Island, SW Finland. Radiocarbon 49(1):47–67.

Marzaioli F, Lubritto C, Nonni S, Passariello I, Capano M, Ottaviano L, Terrasi F. 2014. Characterisation of a new protocol for mortar dating: [14]C evidences. Open Journal of Archaeometry 2(2):55–59.

Michalska D. 2019. Influence of different pretreatments on mortar dating results. Nuclear Instruments and Methods in Physics Research B 456:236–246.

Michalska D, Czernik J. 2015. Carbonates in leaching reactions in context of ^{14}C dating. Nuclear Instruments and Methods in Physics Research B 361:431–439. doi: 10.1016/j.nimb.2015.08.033.

Miriello D, Barca D, Bloise A, Ciarallo A, Crisci GM, De Rose T, Gattuso C, Gazineo F, La Russa MF. 2010. Characterisation of archaeological mortars from Pompeii (Campania, Italy) and identification of construction phases by compositional data analysis. Journal of Archaeological Science 37(9):2207–2223. doi: 10.1016/j.jas.2010.03.019.

Nawrocka D, Michniewicz J, Pawlyta J. 2005. Application of radiocarbon method for dating of lime mortars. Geochronometria 24: 109–115.

Poduska KM, Regev L, Boaretto E, Addadi L, Weiner S, Kronik L, Curtarolo S. 2011. Decoupling local disorder and optical effects in infrared spectra: differentiating between calcites with different origins. Advanced Materials 23: 550–554.

Ponce-Antón G, Ortega L, Zuluaga M, Alonso-Olazabal A, Solaun J. 2018. Hydrotalcite and hydrocalumite in mortar binders from the medieval castle of Portilla (Álava, North Spain): accurate mineralogical control to achieve more reliable chronological ages. Minerals 8(8):326. doi: 10.3390/min8080326.

Porath Y. 2008. Caesarea. The Israel Antiquities Authority excavations. In: Stern E, Geva H, Paris A, editors. The new encyclopedia of archaeological excavations in the Holy Land. Supplement Vol. 5. Jerusalem. p.1656–1665.

Raban A. 2009. Underwater excavations in the Herodian harbor Sebastos. In: Holum KG, Stabler JA, Reinhard EG, editors. Caesarea reports and studies: excavations 1995–2007 within the Old City and the Harbor. BAR International Series 1784: 129–142.

Reinhard EG, Raban A. 2009. Site formation and stratigraphic development of the ancient harbor at Caesarea Maritima, Israel. In: Holum KG, Stabler JA, Reinhard EG, editors. Caesarea reports and studies: excavations 1995–2007 within the Old City and the Harbor. BAR International Series 1784:155–182.

Regev L, Poduska KM, Addadi L, Weiner S, Boaretto E. 2010. Distinguishing between calcites formed by different mechanisms using infrared spectrometry: archaeological applications. Journal of Archaeological Science 37 (12): 3022–3029.

Regev L, Eckmeier E, Mintz E, Weiner S, Boaretto E. 2011. Radiocarbon concentrations of wood ash calcite: potential for dating. Radiocarbon 53(1):117–127.

Ricci G, Secco M, Marzaioli F, Terrasi F, Passariello I, Addis A, Lampugnani P, Artioli G. 2020. The Cannero Castle (Italy): development of radiocarbon dating methodologies in the framework of the layered double hydroxide mortars. Radiocarbon 62. In this issue.

Rietveld H. 1969. A profile refinement method for nuclear and magnetic structures. Journal of Applied Crystallography 2:65–71.

Ringbom Å, Lindroos A, Heinemeier J, Sonck–Koota P. 2014. 19 years of mortar dating: learning from experience. Radiocarbon 56:619–635.

Rowe H, Hughes N, Robinson K. 2012. The quantification and application of handheld energy-dispersive X-ray fluorescence (ED-XRF) in mudrock chemostratigraphy and geochemistry. Chemical Geology 324:122–131.

Secco M, Dilaria S, Addis A, Bonetto J, Artioli G, Salvadori M. 2018. The evolution of the Vitruvian recipes over 500 years of floor-making techniques: The case studies of the Domus delle Bestie Ferite and the Domus di Tito Macro (Aquileia, Italy). Archaeometry 60(2):185–206. doi: 10.1111/arcm.12305.

Snellings R, Mertens G, Elsen J. 2012. Supplementary cementitious materials, reviews in mineralogy and geochemistry. Appl. Mineral. Cement Concrete 74(1): 211–278.

Sonninen E, Jungner H. 2001. An improvement in preparation of mortar for radiocarbon dating. Radiocarbon 43(2):271–273.

Stabler JA, Holum KG, Stanley FH Jr, Risser M, Iamim A. 2008. The Warehouse Quarter (Area LL) and the Temple Platform (Area TP), 1996–2000 and 2002 Seasons. In: Holum KG, Stabler JA, Reinhard EG, editors. Caesarea reports and studies: excavations 1995–2007 within the Old City and the Harbor. BAR International Series 1784:1–40.

Suzuki M, Dauphin Y, Addadi L, Weiner S. 2011. Atomic order of aragonite crystals formed by mollusks. CrystEngComm 13(22):6780–6786.

Toffolo MB, Regev L, Dubernet S, Lefrais Y, Boaretto E. 2019. FTIR-based crystallinity

assessment of aragonite-calcite mixtures in archaeological lime binders altered by diagenesis. Minerals 9(2):121.

Van Strydonck M. 2016. Radiocarbon dating of lime mortars: A historic overview. In: 4th Historic Mortars Conference HMC2016. p. 648–655.

Vola G, Gotti E, Brandon C, Oleson JP, Hohlfelder RL. 2011. Chemical, mineralogical and petrographic characterization of Roman ancient hydraulic concretes cores from Santa Liberata, Italy, and Caesarea Palestinae, Israel. Periodico di mineralogia, 80(2):317–338.

Zouridakis N, Saliege JF, Person A, Filippakis SE. 1987. Radiocarbon dating of mortars from ancient Greek palaces. Archaeometry 29(1): 60–68.